

Temperature Dependent Empirical Pseudopotential Theory For Self-Assembled Quantum Dots

Jianping Wang,¹ Ming Gong,^{2,*} Guang-Can Guo,¹ and Lixin He^{1,†}

¹*Key Laboratory of Quantum Information, University of Science and Technology of China, Hefei, 230026, People's Republic of China*

²*Department of Physics and Astronomy, Washington State University, Pullman, Washington, 99164 USA*
(Dated: September 21, 2018)

We develop a temperature dependent empirical pseudopotential theory to study the electronic and optical properties of self-assembled quantum dots (QDs) at finite temperature. The theory takes the effects of both lattice expansion and lattice vibration into account. We apply the theory to the InAs/GaAs QDs. For the unstrained InAs/GaAs heterostructure, the conduction band offset increases whereas the valence band offset decreases with increasing of the temperature, and there is a type-I to type-II transition at approximately 135 K. Yet, for InAs/GaAs QDs, the holes are still localized in the QDs even at room temperature, because the large lattice mismatch between InAs and GaAs greatly enhances the valence band offset. The single particle energy levels in the QDs show strong temperature dependence due to the change of confinement potentials. Because of the changes of the band offsets, the electron wave functions confined in QDs increase by about 1 - 5%, whereas the hole wave functions decrease by about 30 - 40% when the temperature increases from 0 to 300 K. The calculated recombination energies of exciton, biexciton and charged excitons show red shifts with increasing of the temperature, which are in excellent agreement with available experimental data.

PACS numbers: 68.65.Hb, 73.22.-f, 78.67.Hc

I. INTRODUCTION

During the past two decades, enormous progress has been achieved in understanding the electronic and optical properties of self-assembled quantum dots (QDs) both through theory and experiments, stimulated by their potential applications in QDs laser at room temperature,¹⁻³ and as qubits and quantum photon emitters at low temperature.⁴⁻⁸ For the former applications, it generally requires high density and highly uniform QDs. The QD laser has been demonstrated with much lower threshold current J_c and much higher material and differential gains as compared to the semiconductor quantum well lasers.⁹ For the latter applications, the preparation of single QD is crucial. A number of methods have demonstrated the feasibility to isolate single QD from QDs ensemble.¹⁰⁻¹³ Rabi oscillation of exciton and charged exciton^{14,15} in single QD have been observed experimentally, showing that the charge and spin quantum states in single QD can be coherently controlled via optical method. The single and entangled photon emission from single QD have also been demonstrated experimentally,¹⁶ that are much brighter¹⁷ than the traditional parameter-down entangled photon source.^{18,19} These experimental achievements pave the way for future application of QDs in quantum computation.

On the other hand, the development of the atomistic theories, including the empirical pseudopotential method²⁰⁻²² and the tight-binding models²³⁻²⁵ provide deep insight to the electronic and optical properties of self-assembled QDs. The atomistic theories of QDs not only give results that agree well with experiments,²⁶⁻²⁹ but also greatly improve our understanding of the prop-

erties of QDs. The atomistic models capture the correct point group symmetry of the QDs, which is missing in the continuum model. Therefore they can give correct interpretation of some subtle properties of the QDs, e.g., the fine structure splitting (FSS),³⁰ and light polarization of excitation.³¹ Unfortunately, so far all the theories of QDs have been restricted to zero temperature.

Temperature is a very important degree of freedom in experiments to tune the electronic and optical properties of QDs. For example, in QDs laser, the temperature has been used to tune the laser wavelength.¹⁻³ In the QD-cavity system, the temperature is generally used to tune the resonance between the QDs and the cavity in order to achieve strong coupling between the two quantum systems.³²⁻³⁵ The temperature dependent optical spectra of (single and ensemble) QDs have been investigated intensively in experiments in the past decades.^{10-12,14,15,36,36-38} New physics, for example, the formation of excitonic polaron^{37,39,40} which is due to strong coupling between exciton and optical phonons, may be found in QDs at high temperature. However, a theoretical understanding of the temperature effects in QDs is still missing. Therefore, to facilitate the future device applications of QDs, the development of a temperature dependent theory is not only of theoretical interest, but also of practical importance.

In this work, we develop such a temperature dependent atomistic pseudopotential theory to study the electronic and optical properties of QDs at finite temperature. We take the effects of both lattice expansion and lattice vibration into account. The latter is done by introducing a temperature dependent dynamical Debye-Waller factor to the structure factor. We first examine

the temperature dependent electronic structures of bulk InAs and GaAs, and then apply the theory to investigate the electronic and optical properties of self-assembled InAs/GaAs QDs. The calculated temperature dependent photoluminescence (PL) spectra of QDs are in excellent agreement with available experimental data.

The rest of the paper is organized as follows. In Sec. II we introduce the temperature dependent empirical pseudopotential method (TDEPM). In Sec. III, we study the electronic structures of bulk InAs, GaAs using TDEPM, including the energy band gaps and band offsets, etc. We present the temperature dependent band offsets for InAs/GaAs QDs in Sec. IV A and the single particle energy levels and wave functions of InAs/GaAs QDs in Sec. IV B. We discuss the temperature dependent optical spectra of InAs/GaAs QDs in Sec. IV C, and summarize in Sec. V.

II. METHODOLOGY

We consider InGaAs QDs embedded in the center of a $60 \times 60 \times 60$ GaAs 8-atom unit cell. Periodic boundary condition is used to obtain the single particle energy levels. To study the electronic and optical properties of the QDs at finite temperature, we introduce temperature dependent pseudopotentials in the single-particle Hamiltonian,

$$\hat{H} = -\frac{1}{2}\nabla^2 + \sum_{n\alpha} \hat{v}_\alpha(\mathbf{r} - \mathbf{R}_{n\alpha}, \epsilon, T), \quad (1)$$

where $\hat{v}_\alpha(\mathbf{r}, \epsilon, T)$ is the strain dependent screened empirical pseudopotential for atom of type α and atom index n at temperature T . $\mathbf{R}_{n\alpha}$ is the optimized atom position from valance force field (VFF) method.^{41,42} In a strained lattice, the atomic potential is assume to have the form of,

$$v_\alpha(\mathbf{r}, \epsilon, T) = v_\alpha(\mathbf{r}, T)[1 + \gamma_\alpha \text{Tr}(\epsilon(\mathbf{r}))], \quad (2)$$

where $\text{Tr}(\epsilon(\mathbf{r}))$ is the local hydrostatic strain at \mathbf{r} . γ_α is fitted to the deformation potentials of the bulk materials. The atomistic theory naturally captures the correct point group symmetry of the QDs even at high temperature.

The effects of lattice vibration can be taken into account using Brooks-Yu theory,⁴⁴ which has been applied to study the energy gap of bulk materials in the context of pseudopotentials.⁴⁵⁻⁴⁸ The total atomic potential at temperature T , which is the sum of all atomic potentials $\hat{v}_\alpha(\mathbf{r}, \epsilon, T)$, can be written as,

$$\begin{aligned} V(\mathbf{r}, T) &= \left\langle \sum_{\mathbf{q}} \sum_{\alpha} v_\alpha(\mathbf{q}) S(\mathbf{q}) e^{i\mathbf{q} \cdot \mathbf{r}} \right\rangle_T \\ &= \sum_{\mathbf{q}} \sum_{\alpha} v_\alpha(\mathbf{q}) \langle S(\mathbf{q}) \rangle_T e^{i\mathbf{q} \cdot \mathbf{r}} \end{aligned} \quad (3)$$

where \mathbf{q} is the reciprocal lattice vector. $v_\alpha(\mathbf{q})$ is the Fourier transform of the screened atomistic potential at

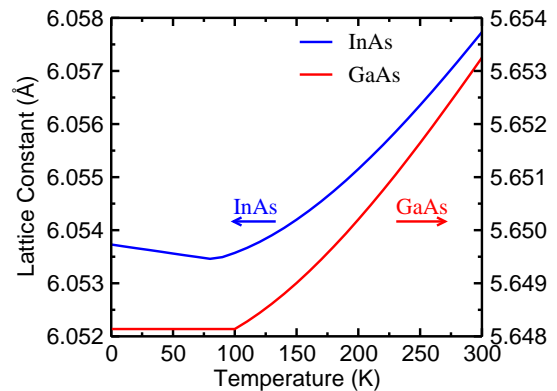


FIG. 1: (color online) Experimental temperature dependent lattice constants for InAs and GaAs. The data are taken from Ref. 43.

zero temperature, which takes the form of,⁴⁹

$$v_\alpha(q) = \frac{\alpha_0(q^2 - \alpha_1)}{\alpha_2 e^{\alpha_3 q^2} - 1} \quad (4)$$

where $q = |\mathbf{q}|$, and the parameters α_0 , α_1 , α_2 , α_3 are fitted to the bulk properties of InAs and GaAs, including the band gaps, band offsets, effective masses, etc. $\langle S_\alpha(\mathbf{q}) \rangle_T$ is the averaged structure factor over all the phonon configurations at temperature T ,

$$\langle S_\alpha(\mathbf{q}) \rangle_T = \left\langle \sum_n e^{-i\mathbf{q} \cdot \mathbf{R}_{n\alpha}} \right\rangle_T. \quad (5)$$

Assuming $\mathbf{R}_{n\alpha} = \mathbf{R}_{n\alpha}^0 + \mathbf{u}_\alpha$, where \mathbf{u}_α is the amplitude of the phonon mode. For any \mathbf{q} , we have

$$\langle e^{-i\mathbf{q} \cdot \mathbf{u}_\alpha} \rangle_T = e^{-\frac{1}{2} \langle (\mathbf{q} \cdot \mathbf{u}_\alpha)^2 \rangle_T}. \quad (6)$$

using Wick's theorem.⁵⁰ Therefore, the temperature effects to the atomic potentials are equivalent to consider a temperature dependent structure factor,

$$\langle S_\alpha(\mathbf{q}) \rangle_T = \sum_n e^{-i\mathbf{q} \cdot \mathbf{R}_{n\alpha}^0} e^{-W_\alpha(\mathbf{q}, T)}, \quad (7)$$

in Eq. 3, where $W_\alpha(\mathbf{q}, T)$ is the dynamical Debye-Waller factor for the α -th element,

$$2W_\alpha(\mathbf{q}, T) = \langle (\mathbf{q} \cdot \mathbf{u}_\alpha)^2 \rangle_T. \quad (8)$$

For simplicity, we assume the system to be isotropic, then we have

$$W_\alpha(\mathbf{q}, T) = \frac{1}{6} |\mathbf{q}|^2 \langle u_\alpha^2 \rangle, \quad (9)$$

where $\langle u_\alpha^2 \rangle$ is the total mean-square displacement for atom of type α at temperature T , including the contribution from acoustic (A) and optical (O) phonons,

$$\langle u_\alpha^2 \rangle = \langle u_\alpha^2 \rangle_A + \langle u_\alpha^2 \rangle_O. \quad (10)$$

We use Debye model for acoustic phonons,

$$\begin{aligned} \langle u^2 \rangle_A &= \int_0^{\omega_D} g(\omega) \frac{\hbar}{NM\omega} \left(\frac{1}{e^{\hbar\omega/k_B T} - 1} + \frac{1}{2} \right) d\omega \\ &= \alpha_4 \left[\left(\frac{T}{\theta_D} \right)^2 \int_0^{\frac{\theta_D}{T}} \frac{x}{e^x - 1} dx + \frac{1}{4} \right], \end{aligned} \quad (11)$$

where $\alpha_4 = 9\hbar/M\omega_D$, and $\theta_D = \hbar\omega_D$ is the Debye temperature. The second term in the bracket is from zero point quantum fluctuation, which can be absorbed to the zero-temperature pseudopotentials. At high temperature, the acoustic phonon displacement $\langle u^2 \rangle_A \propto T$, whereas in the low-temperature limit, $\langle u^2 \rangle_A \propto T^2$. For the optical phonons, the average displacement can be written as

$$\langle u^2 \rangle_O = \frac{\alpha_5}{e^{\hbar\omega_O/K_B T} - 1}, \quad (12)$$

where ω_O is the frequency of the optical phonon. We neglect the dispersion of optical phonons here. Generally, the contribution of the optical phonon could be significant only at high temperature.⁵¹ Although α_4 and α_5 can be calculated directly using the parameters of bulk materials, the approximations made during the derivations of Eq. (11) and (12) can introduce some errors to the energy gap of semiconductors at finite temperature. To overcome this problem, we treat α_4 and α_5 as fitting parameters, which are fitted to the temperature dependent band structures in combination with the zero-temperature empirical pseudopotentials. Therefore, the dynamical Debye-Waller factors might be different from the real physical Debye-Waller factors of the system.

TABLE I: Band parameters obtained from the empirical pseudopotential calculations compared with the experimental values.^{52,53} Energies are in unit of eV. m_e^* , $m_{hh}^*[100]$, $m_{hh}^*[111]$ and $m_{lh}^*[100]$ are effective masses of electron and holes at Γ point. a_{gap} and $a_{\Gamma_{15v}}$ denote the deformation potential of the band gap and the Γ_{15v} point. b is the valance band biaxial deformation potential. Δ_0 and Δ_1 are the spin-orbit splittings at the Γ_{15v} and L_{1v} points respectively.

Property	GaAs		InAs	
	EPM	Expt.	EPM	Expt.
E_{gap}	1.528	1.52	0.423	0.42
$E_{X_{5v}}$	-2.763	-2.96	-2.365	-2.40
$E_{X_{1c}}$	1.937	1.98	2.069	2.34
$E_{X_{3c}}$	2.232	2.50	2.514	2.54
$E_{L_{3v}}$	-1.041	-1.30	-0.872	-1.26
$E_{L_{1c}}$	2.232	1.81	1.568	1.71
m_e^*	0.067	0.067	0.023	0.023
$m_{hh}^*[100]$	0.316	0.40	0.371	0.35
$m_{hh}^*[111]$	0.825	0.57	0.986	0.85
$m_{lh}^*[100]$	0.092	0.082	0.029	0.026
a_{gap}	-7.879	-8.33	-6.804	-5.7
$a_{\Gamma_{15v}}$	-1.110	-1.0	-0.829	-1.0
b	-1.567	-1.7	-1.631	-1.7
Δ_0	0.362	0.34	0.384	0.39
Δ_1	0.201	0.22	0.286	0.27

TABLE II: Fitted pseudopotential parameters for InAs/GaAs in Eq.(2) and Eq.(4). A plane-wave cutoff of 5 Ryd is used.

parameters	Ga	As (GaAs)	In	As (InAs)
α_0	476845.70	11.9753	771.3695	26.8882
α_1	1.9102	3.0181	1.6443	2.9716
α_2	22909.50	1.1098	18.1342	1.2437
α_3	0.1900	0.2453	0.3940	0.4276
γ_α	2.5215	0.0	2.1531	0.0
α_{so}	0.1035	0.0976	0.5973	0.0976

TABLE III: Debye temperatures,⁵³ the optical phonon energies and the fitted α_4 , α_5 parameters for GaAs and InAs.

Bulk	θ_D (K)	ω_O (meV)	cation		anion	
			α_4	α_5	α_4	α_5
GaAs	344	35.36	0.3024	0.0786	0.1530	0.0024
InAs	247	29.6	0.1014	0.0984	0.0828	0.0084

To determine the temperature dependent pseudopotential, we first determine the pseudopotential parameters $\alpha_0 - \alpha_3$ and γ at zero temperature by fitting them to the electronic structures of bulk materials, including the effective mass, and energies of the high symmetry Γ , X and L points, etc. The target values and fitted values for GaAs and InAs are compared in Table I, which are in good agreement. The parameters $\alpha_0 - \alpha_3$ and γ are presented in Table II. With these parameters at hand, we then determine the values of α_4 and α_5 by fitting them to the temperature dependent energy gap of bulk materials, which can be well described by the empirical Varshni formula,^{52,54}

$$\Delta E_g(T) = -\frac{c_1 T^2}{T + c_2}, \quad (13)$$

where c_1 and c_2 are the Varshni parameters. For GaAs, $c_1 = 0.5405$ meV/K and $c_2 = 204$ K and for InAs, $c_1 = 0.276$ meV/K and $c_2 = 93$ K.⁵² The fitted parameters for α_4 and α_5 are summarized in Table. III.

The single-particle Hamiltonian (1) can be solved by expanding the wave functions into a linear combination of Bloch bands (LCBB),²²

$$\psi_i = \sum_{n,\mathbf{k},\lambda} c_{n,\mathbf{k},\lambda}^i \psi_{n,\epsilon,\mathbf{k},\lambda,T}, \quad (14)$$

where $\psi_{n,\epsilon,\mathbf{k},\lambda,T}$ is the bulk Bloch bands with orbital n and wave vector \mathbf{k} close to Γ point at finite temperature T , and $\lambda = (\text{InAs}, \text{GaAs})$. The experimental lattice constants for InAs and GaAs at given temperature, as shown in Fig. 1, are given as input to construct the Bloch basis. At each temperature, we relax the dot+matrix structure using VFF method to get the the atomic position $\mathbf{R}_{n,\alpha}(T)$.

Due to the spatial confinement, the carries in the QDs have strong Coulomb interactions. The many-particle

Hamiltonian read as,

$$H = \sum_i \epsilon_i \hat{\psi}_i^\dagger \hat{\psi}_i + \frac{1}{2} \sum_{ijkl} \Gamma_{ij}^{kl} \hat{\psi}_i^\dagger \hat{\psi}_j^\dagger \hat{\psi}_k \hat{\psi}_l, \quad (15)$$

where $\hat{\psi}_i = c_i \psi_i(\mathbf{r})$ is the field operator with corresponding single particle energy ϵ_i . Γ_{ij}^{kl} are the Coulomb integrals,

$$\Gamma_{ij}^{kl} = \int \int d\mathbf{r} d\mathbf{r}' \frac{\psi_i^*(\mathbf{r}) \psi_j^*(\mathbf{r}') \psi_k(\mathbf{r}') \psi_l(\mathbf{r})}{\epsilon(\mathbf{r} - \mathbf{r}') |\mathbf{r} - \mathbf{r}'|}. \quad (16)$$

Here, $\epsilon(\mathbf{r} - \mathbf{r}')$ is the screened dielectric function.⁵⁵ The many-particle Hamiltonian is solved using a configuration interaction method,⁵⁶ where the many-particle wave functions are expanded on the Slater determinants constructed from the confined electron and hole levels. This method has been successfully applied to studying the electronic and optical properties of InAs/GaAs QDs and the obtained results are in very good agreement with the experimental observations.^{26,28,29,49}

III. TDEPM FOR BULK MATERIALS

We first test our method for bulk materials. Figure 2 depicts typical band structures of GaAs at $T = 0$ and $T = 300$ K. The overall band structures are quite similar to those at zero temperature even at rather high temperature (300 K). However, the energies of high symmetry k -points Γ , X , and L have different response to the temperature. In principle, all the energies of these k -points should be taken as the target values to determine the values of α_4 and α_5 . Unfortunately, the experimental data of the energies of these k -points at finite temperature are not available, therefore, tentatively, we fit the potentials only to the temperature dependent energy gaps at Γ point. The potentials can be improved by fitting to the energies of more k -points in the future.

We present in Fig. 3 the change of energy gap ΔE_g as a function of temperature for GaAs. The filled circles are the results taken from experiments,⁵² whereas the solid line is calculated from TDEPM. The fitting error is less than 0.2 meV in the whole temperature range. The dashed line is the change of energy gap of GaAs taken account only lattice vibration, whereas the dotted line is the result with only lattice expansion. As we see, to accurately describe the red shift of the band gap with respect to temperature, both the lattice expansion and lattice vibration have to be taken into account in the theory. These results agree with the results obtained from temperature dependent tight-binding method by Pour et al.⁵⁷ Similar features are also found for InAs using the parameters given in Table III.

The conduction band offset (ΔE_c) and valance band offset (ΔE_v) between InAs and GaAs, defined as

$$\begin{aligned} \Delta E_c &= E_{\Gamma}^{\text{CBM}}(\text{GaAs}) - E_{\Gamma}^{\text{CBM}}(\text{InAs}), \\ \Delta E_v &= E_{\Gamma}^{\text{VBM}}(\text{InAs}) - E_{\Gamma}^{\text{VBM}}(\text{GaAs}), \end{aligned} \quad (17)$$

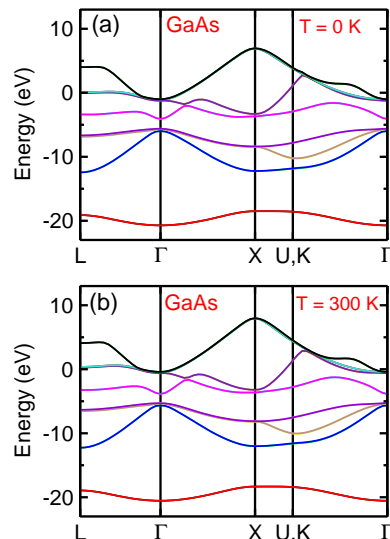


FIG. 2: (color online) The band structures of GaAs at $T = 0$ (a) and $T = 300$ K (b) calculated by the TDEPM.

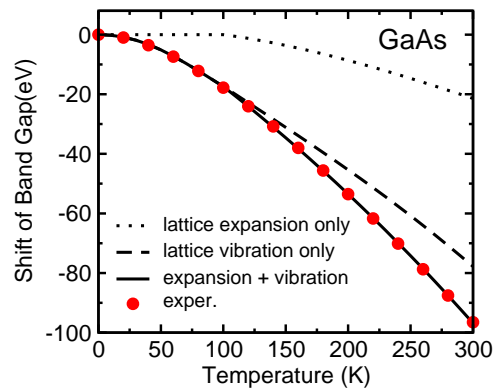


FIG. 3: (color online) The red shift of band gap as a function of temperature for GaAs. The filled circles represent the experimental data. The dashed line is the result calculated from TDEPM with only lattice vibration whereas the dotted line is the result with only lattice expansion. The solid line is from TDEPM taking account of both lattice vibration and lattice expansion.

are very important to the electronic structures of the InAs/GaAs heterostructures, because they are important for the confinement of electron and hole in InAs/GaAs QDs. We show the change of CBM and VBM of InAs and GaAs with temperature in Fig. 4 (a), and the temperature dependent band offsets between InAs and GaAs in Fig. 4 (b). We find:

(i) The CBM and VBM of GaAs change much larger than their counterparts in InAs.

(ii) The CBM generally changes much larger than VBM. At high temperature ($T > 100$ K), CBM and VBM change approximately linearly with respect to temperature. The changes of the band offsets with respect to the temperature are presented in Fig. 4 (b) for the VBM and in the inset for CBM. For electron, the temperature effect

generally enhances the band offset, whereas for hole, the band offset decreases with the increasing of the temperature. Interestingly, there is a type-I to type-II transition at $T = 135$ K for unstrained InAs/GaAs. However, because of the strain effects, the holes are still localized in InAs/GaAs QDs (see Sec. IV). In what follows we will show that the change of band offsets at finite temperature will greatly modify the electronic and optical properties of QDs.

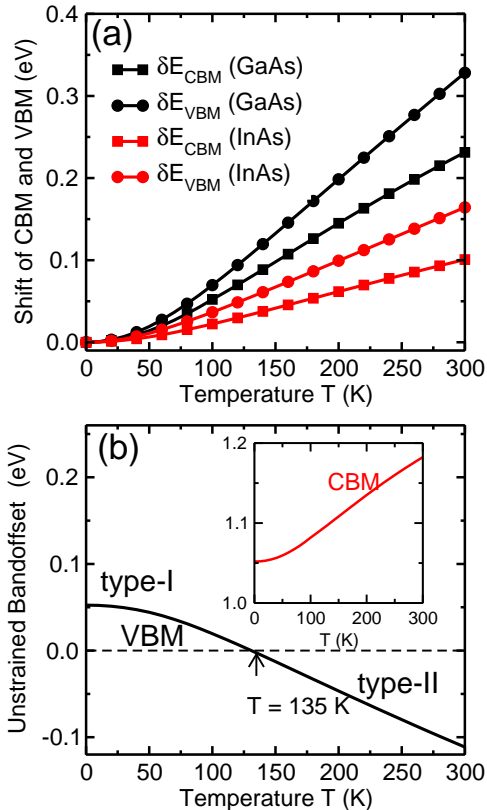


FIG. 4: (color online) (a) Changes of CBM and VBM as functions of temperature for InAs and GaAs bulk materials. (b) The valence band offset and the conduction band offset (inset) between InAs and GaAs as functions of temperature.

IV. TDEPM FOR INAS/GAAS QDS

In Sec. III, we study the temperature dependent electronic structures of bulk InAs and GaAs. The band offsets between InAs and GaAs are greatly modified due to the temperature effects and there is a type-I to type-II transition in the unstrained InAs/GaAs heterostructure. The change of band offsets will significantly change the corresponding electronic and optical properties in QDs. However, the temperature dependent properties are more complicated in QDs because of the strain effects. In this section, we investigate the temperature dependent electronic and optical properties of InAs/GaAs QDS using TDEPM. We study QDs with different sizes and alloy

TABLE IV: The alloy composition and size of the lens shaped $\text{In}_x\text{Ga}_{1-x}\text{As}/\text{GaAs}$ QDs used in this work.

#	x	Base (nm)	Height (nm)
QD-A	1.0	25	3.5
QD-B	0.6	25	3.5
QD-C	0.7	25	3.5
QD-D	0.8	25	3.5
QD-E	1.0	25	5.5
QD-F	0.6	25	5.5
QD-G	0.7	25	5.5
QD-H	0.8	25	5.5

compositions. The alloy compositions of selected lens-shaped QDs are presented in Table IV. In most of the cases, we use QD-A to illustrate the main physics. The results of other QDs will also be presented for comparison.

A. Temperature dependent band offset

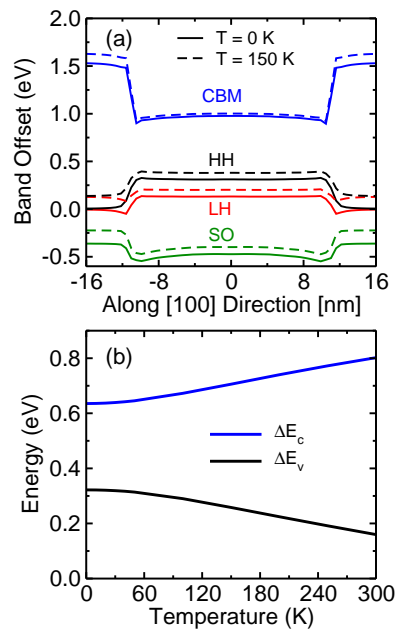


FIG. 5: (color online) (a) Typical band profiles in strained QDs. HH, LH and SO correspond to heavy hole, light hole and spin-orbit bands respectively. (b) The band offsets at the center of InAs/GaAs QDs as functions of temperature calculated from TDEPM.

We first investigate the strained band offsets in InAs/GaAs QDs, which is crucial for the electronic and optical properties of QDs. In previous works,^{58,59} the Bir-Pikus model is used to obtain the strain modified band profiles. However, the temperature dependent parameters for the Bir-Pikus model is generally unavailable. Therefore, we calculate the band profiles directly using the TDEPM. After the lattice relaxations for the dot sys-

tem, we construct the 8-atom unit cell according to the local strain, and then calculate the band structures using the TDEPM. Typical band offsets in InAs/GaAs dots along the [100] direction at $T = 150$ K is compared to those of zero temperature in Fig. 5 (a). We see that the overall profiles of the heavy hole (HH) and light hole (LH) and spin-orbit (SO) bands are still quite similar at the two temperatures. The SO band is lower than the HH and LH by about 400 meV in the matrix and is greatly enhanced in the dot materials. The degeneracy of the HH and LH bands is broken because of the biaxial strain.^{58,60} The strained band offsets of CBM and VBM in the center of InAs/GaAs QDs are presented in Fig. 5 (b) in the temperature range of 0 - 300 K. For electrons, the confinement is enhanced with increasing of the temperature, whereas for holes, the confinement decreases from 320 to 180 meV. However, unlike the bulk materials, even at high temperature, ΔE_v is always positive, indicating that the hole is always localized in the QDs. The change of the band offsets greatly modifies the electronic and optical properties of QDs, as shall be discussed below.

B. Temperature dependent single particle levels and wave functions

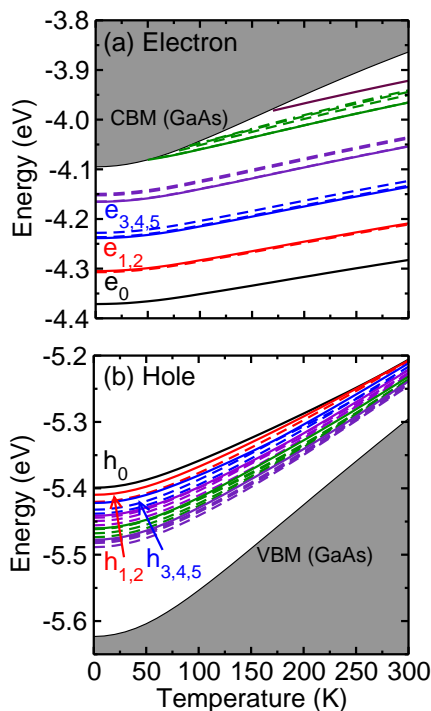


FIG. 6: (color online) Single-particle energy levels of the confined states as functions of temperature in QD-A. The shaded regime at the top (bottom) panel corresponding to the unconfined states with energies higher (lower) than the CBM (VBM) of GaAs.

The evolution of single particle energy levels as func-

tions of temperature is illustrated in Fig. 6. We show the results for QD-A here. Similar features are also found for all other QDs. We show all confined electron states, and the highest 20 hole states. Because of the enhancement of confinement potential for electrons, more states are confined in the dots as the increasing of the temperature. The labels of e_i (h_i) represent the energy levels of electron (hole) in ascending (descending) order. One can also use angular momentum s , p , d , etc. to label the wave functions. For instance, the states e_0 and h_0 can be labeled as s and the $e_{1,2}$ ($h_{1,2}$) states are usually labeled by $p_{1,2}$, etc.

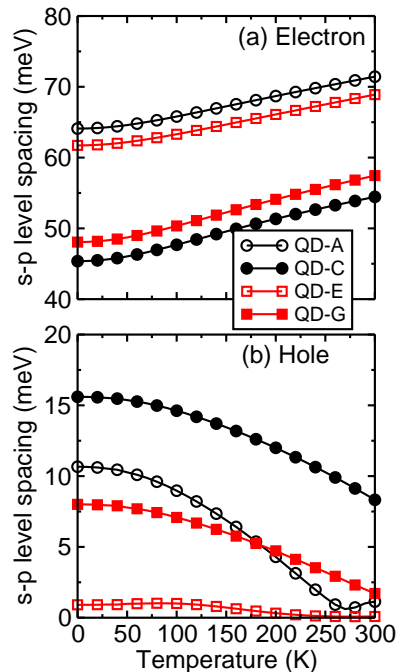


FIG. 7: (color online) The single-particle s - p level energy spacing as functions of temperature for electrons and holes in the InAs/GaAs QDs.

The s - p energy level spacing is shown in Fig. 7, which is defined as,

$$\delta\epsilon_{sp} = \left| \frac{\epsilon_{p_1} + \epsilon_{p_2}}{2} - \epsilon_s \right| \quad (18)$$

for both electrons and holes. Because of the increase of confinement potential, the electron s - p level spacing increases with the increasing of the temperature. In contrast, for holes, the energy level spacings decreases with the increasing of the temperature due to the decrease of the hole confinement potential. For QD-A, we find that the level spacing of electron increases from 64 to 70 meV when the temperature increases from 0 K to 300 K. For hole, the energy difference decreases from 11 to about 1 meV. The change of level spacings in QDs may be measured from PL emission spectra.

The p -orbital splitting is another important quantity for

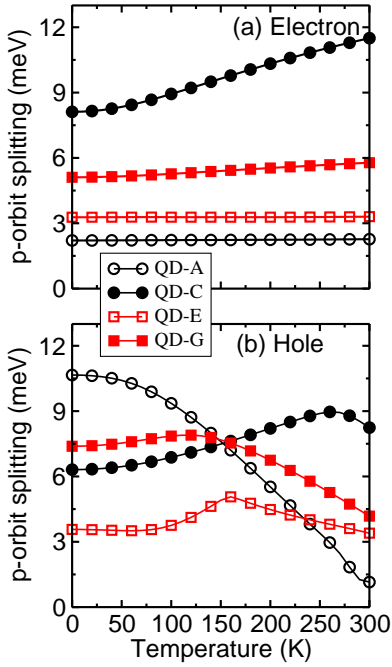


FIG. 8: (color online) The single-particle p -orbit energy splittings as a functions of temperature for electrons and holes in InAs/GaAs QDs.

the single particle levels, which is defined as,

$$\delta\epsilon_{pp} = |\epsilon_{p1} - \epsilon_{p2}|.$$

If the QDs have C_{4v} or T_d symmetry, the p -orbit splitting is exactly zero. However, for real QDs, the highest symmetry is C_{2v} , and in alloyed QDs, the symmetry is C_1 , the splitting is nonzero. The results of the p -orbit splittings are presented in Fig. 8 for different types of QDs. For QD-A and QD-E, the electron p -orbit splittings are almost independent of temperature, whereas for other two types of QDs the p -orbit splittings slightly increase with the increasing of temperature. The results for holes are very different from those for electrons, as shown in Fig. 8 (b). Because the hole level spacings are very small and the anti-crossing between the hole levels may occur when increasing the temperature, the p -level splittings are not monotonic functions of the temperature. At high temperature, the p -level spacing may even exceed the s - p level spacing, which will never happen for electrons. The p -orbit splitting can be measured experimentally via pump-probe spectroscopy.^{61,62}

The change of confinement potentials may also change the shapes of the wave functions. We present the squared envelope wave functions of electrons and holes at $T = 0, 100$ and 300 K in Fig. 9 for QD-A. The number on the lower right corner of each small panel represents the percentage of the density confined in the QDs. For $e_{0,1,2}$, we find that the confined densities increase by about 1% - 2%, whereas for the higher states, the confined densities may increase about 4% - 5%. Although the electron squared wave functions confined in QDs slightly increase,

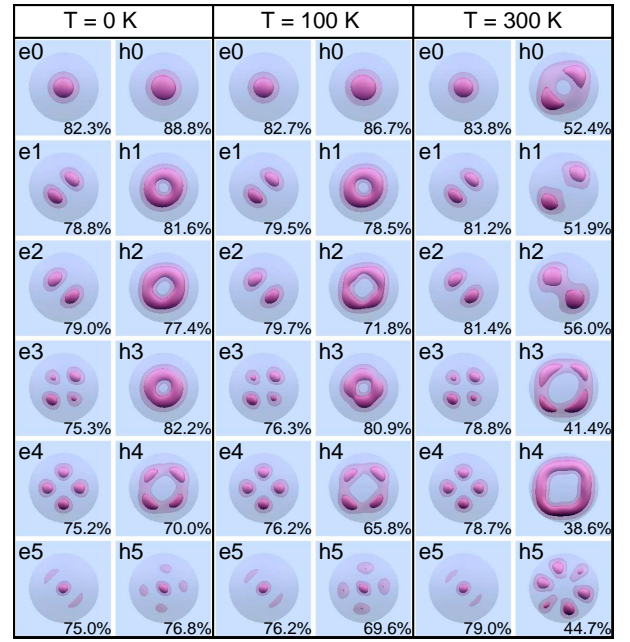


FIG. 9: (color online) The squared envelope wave functions of the confined electron and hole states at $T = 0$ K, 100 K and 300 K. The number on the lower right corner of each small panel represents the percentage of the state densities confined in the QDs.

their overall shapes hardly change. In contrast, for holes, the confined densities reduce dramatically when the temperature increases. For instance, the confined density decreases from 88.8% to 52.4% for h_0 when the temperature increases from 0 to 300 K. For h_5 , the confined density decreases from 76.8% to 44.7%. The shapes of the envelope functions for holes also change dramatically. For instance, the h_0 state is Gaussian-like at low temperature, but at high temperature there is a node at the center of the wave function. This change of the wave function is due to the enhancement of the interfacial effect in the QDs, because the confinement is very small for holes at high temperature. At low temperature only the tall QDs have such interfacial hole states.^{58,59} The change of the wave functions with respect to temperature can be measured experimentally using magnetotunneling spectroscopy.^{63,64}

C. Temperature dependent PL emission spectrum

In this section, we investigate the temperature dependence of the optical spectra of InAs/GaAs QDs. The optical spectra of single InAs/GaAs QD^{10-12,14,15,36} have been measured at low temperature. The highest measuring temperature as far as we know is up to 100 K, performed by Ortner *et al.*³⁶ At higher temperature, the signal to noise ratio may become very low and the single QD emission is usually hard to detect. However, for QDs

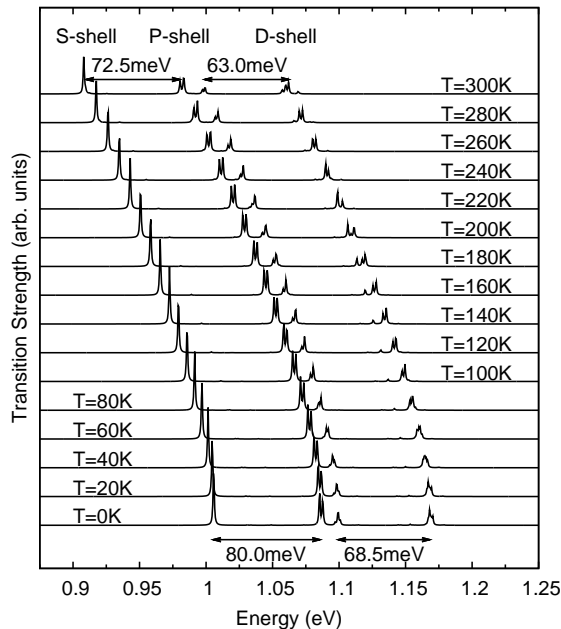


FIG. 10: Temperature dependent PL emission spectra of QD-A. The emission lines are broadened by 0.5 meV with a Lorentz function.

ensemble, the emissions from QDs can be resolved even at room temperature. Therefore in this work, we study the optical spectra of QDs up to 300 K.

Figure 10 depicts the PL emission spectra of QD-A from 0 K to 300 K. The energy difference between S and P shell emission can be approximated by the sum of s - p single particle energy level spacing of electron and hole, i.e.

$$\Delta E_{SP} \approx \delta\epsilon_{sp}^e + \delta\epsilon_{sp}^h.$$

Although the change of level spacing in Fig. 7 can not be directly measured from PL emission spectra, the sum of them can be measured. The energy difference between S and P shells for QD-A is 80 meV at zero temperature and reduces to 72.5 meV at 300 K.

Figure 11 depicts the temperature dependent energies of the primary exciton, biexciton and charged excitons for dots A, C, E, G. All the energies of exciton complexes show red shift as the temperature increases. For all dots, we find that the red shifts of the exciton complexes emission lines can be fitted very well using Varshni formula, with the fitting errors generally less than 1 meV. The fitting errors are slightly larger than that for the bulk materials (< 0.2 meV), but much smaller than the total red shift of the emission line which is about 100 meV. This suggests that the red shift of the emission energies is proportional to T^2 at low temperature. The values of the Varshni parameters are summarized in Table V. These parameters are very different than those of bulk InAs, GaAs, and also vary from dot to dot.

The temperature dependent optical spectra has been

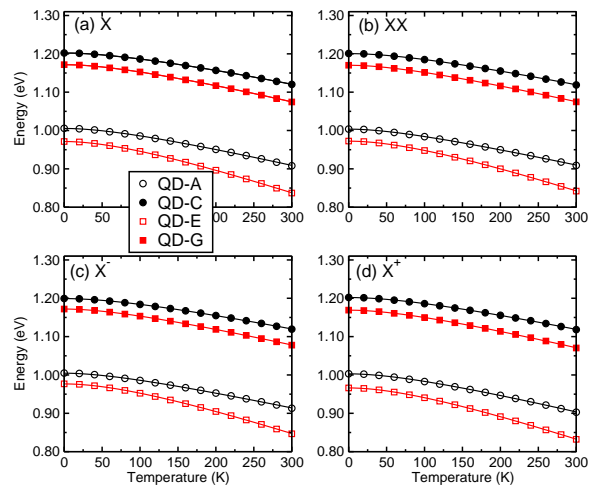


FIG. 11: (color online) The red shifts of emission lines of (a) X, (b) XX, and (c) X^- and (d) X^+ as functions of temperature. The symbols are the results calculated from TDEPM, whereas the solid lines are the fitted results using Varshni formula.

studied experimentally by several groups.^{36,38} For example, red shift of exciton emission line in single QDs have been investigated by Ortner *et al*³⁶ from $T = 0$ K to $T = 100$ K. In Fig. 12 (a), we compare our theoretical results (QD-B, QD-F) with the available experimental data³⁶ for the $\text{In}_{0.6}\text{Ga}_{0.4}\text{As}/\text{GaAs}$ QDs. The red shift of the emission line of exciton agree well with QD-B (less than 1 meV). In the inset of Fig. 12, we present the exciton energies as a functions of temperature, which also show excellent agreement. The red shift of exciton energy in Ref. 36 can be well described by Varshni formula using $c_1 = 0.4419$ meV/K and $c_2 = 221.77$ K, with error less than 1 meV. This is also in a good agreement with the theoretical values for QD-B given in Table V.

In Fig. 12 (b), we compare the theoretical results of QD-A and QD-C with the experimental results for QDs ensemble measured by Yeo *et al*.³⁸ where the peak energy of S -shell is chosen as the exciton emission lines at each temperature. For QDs ensemble, the S -shell can be well resolved even at room temperature. We see that the red shifts of QDs ensemble A_2 and A_3 agree well with the theoretical prediction of QD-A. Moreover, the exciton energy of A_2 and A_3 at zero temperature is around 1.02 - 1.03 eV, also agree well with the exciton energy of QD-A listed in Table V.

We note that some experiments⁶⁵ suggest that the red-shift of the exciton energies proportional to T^4 ,^{66,67} instead of T^2 as suggested by TDEPM at very low temperature ($T < 10$ K). The discrepancy may come from two reasons. First, it is because we do not have high accurate temperature dependent band gaps to fit at very low temperature at present stage. It may also partly comes from the approximations we made in deriving the temperature dependent pseudopotentials. Nevertheless, in this temperature range, the change of exciton energies is

TABLE V: Fitted Varshni parameters for different QDs. E_0 is the energy at zero temperature in unit of eV. The Varshni parameters, c_1 is in unit of meV/K and c_2 is in unit of K. The geometry and alloy composition of the QDs are listed in Table IV.

#	$E_0(X)$	$c_1(X)$	$c_2(X)$	$E_0(XX)$	$c_1(XX)$	$c_2(XX)$	$E_0(X^-)$	$c_1(X^-)$	$c_2(X^-)$	$E_0(X^+)$	$c_1(X^+)$	$c_2(X^+)$
QD-A	1.0056	0.4861	151.2457	1.0038	0.4583	137.7505	1.0048	0.4451	139.6235	1.0031	0.5050	155.5669
QD-B	1.2600	0.4579	231.8752	1.2592	0.4500	217.6022	1.2568	0.4458	229.9588	1.2610	0.4605	217.5235
QD-C	1.2021	0.4419	187.7806	1.2007	0.4364	181.1664	1.1994	0.4266	182.4588	1.2021	0.4493	184.1575
QD-D	1.1109	0.4357	157.3439	1.1392	0.4275	151.4595	1.1387	0.4062	141.2489	1.1399	0.4503	161.8518
QD-E	0.9714	0.7165	180.7079	0.9725	0.7127	193.0234	0.9768	0.7148	195.3687	0.9663	0.7178	182.4702
QD-F	1.2322	0.4957	188.3547	1.2305	0.4854	182.7430	1.2312	0.4836	189.6459	1.2306	0.4994	183.6016
QD-G	1.1717	0.5017	165.5773	1.1702	0.4861	159.2807	1.1720	0.4800	159.7797	1.1691	0.5107	166.9354
QD-H	1.1085	0.5393	164.2455	1.1077	0.5151	155.4030	1.1102	0.5059	153.0005	1.1052	0.5424	161.4847

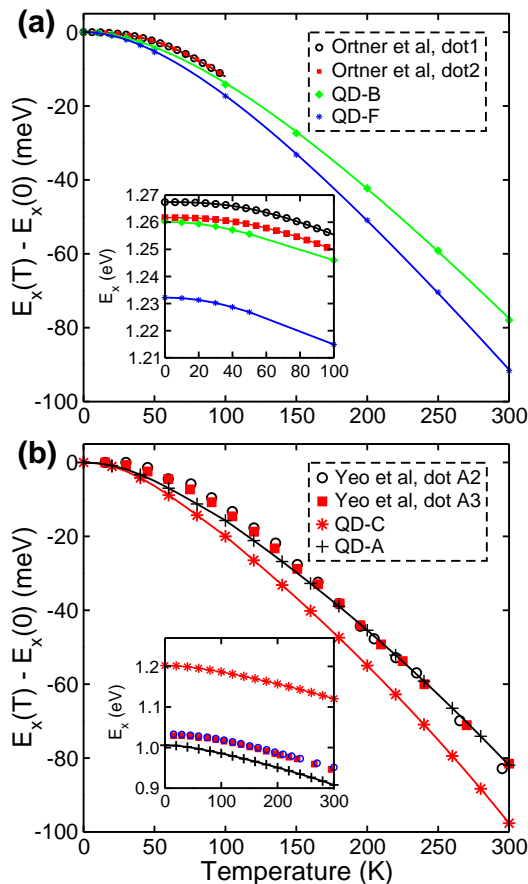


FIG. 12: (color online) (a) Comparison of the red shifts of the exciton emission energies of QD-B and QD-F to the experimental data of single QDs (dot1, dot2) in Ref. 36. (b) Comparison of the red shifts of the exciton emission energies of QD-A and QD-C to the experimental data of QDs ensemble (A_2 , A_3) in Ref. 38. In both figures, the insets depict the exciton energies as functions of temperature.

very small, and the difference between the experimental values and the theory is very subtle.

We also calculate the FSS and the polarization of the mono-exciton at finite temperatures. We find that the FSS and the polarization are generally insensitive to the temperature. For example, the change of FSS is usually

less than $1 \mu\text{eV}$, and the change of polarization is less than 5 degree when increasing the temperature from 0 to 100 K. This result suggests that the FSS can not be tuned using temperature effect.

V. SUMMARY AND CONCLUSIONS

We develop a temperature dependent empirical pseudopotential theory, and apply it to study the electronic and optical properties of self-assembled InAs/GaAs quantum dots (QDs) at finite temperature. The theory takes the effects of both lattice expansion and lattice vibration into account. The pseudopotentials correctly reproduce the temperature dependent band gap of bulk III-V semiconductors such as InAs, and GaAs, etc. We find that for the unstrained InAs/GaAs heterostructure, the conduction band offset increases whereas the valence band offsets decreases with the increasing of the temperature, and there is a type-I to type-II transition at approximately 135 K. Yet, for InAs/GaAs QDs, the holes are still localized in the QDs even at room temperature because the large lattice mismatch between InAs and GaAs greatly enhances the valence band offset. The single particle energy levels in the QDs show strong temperature dependence due to the change of confinement potentials. As a consequence, more electron states are confined at higher temperature. Because of the changes of the band offsets, the electron wave functions confined in QDs increase by about 1 - 5%, whereas the hole wave functions decrease by about 30 - 40% when the temperature increase from 0 to 300 K. The calculated recombination energies of exciton, biexciton and charged excitons show red shift with the increasing of the temperature, which are in excellent agreement with available experimental data. We expect the theory can facilitate the future device applications of QDs.

Acknowledgments. - LH acknowledges the support from the Chinese National Fundamental Research Program 2011CB921200, National Natural Science Funds for Distinguished Young Scholars and the Fundamental Research Funds for the Central Universities No. WK2470000006.

- * Electronic address: gong.skylark@gmail.com.
† Electronic address: helx@ustc.edu.cn.
- ¹ R. Tsu and L. Esaki, *Appl. Phys. Lett.* **22**, 562 (1973).
 - ² Y. Arakawa and H. Sakaki, *Appl. Phys. Lett.* **40**, 939 (1982).
 - ³ N. Kirstaedter, N. N. Ledentsov, M. Grudmann, D. B. V. Ustinov, S. Ruvimov, M. Maximov, P. K. and Z. Alferov, U. Richter, P. Werner, U. Gosele, et al., *Electronics Letters* **30**, 1416 (1994).
 - ⁴ A. Imamoglu and Y. Yamamoto, *Phys. Rev. Lett.* **72**, 210 (1994).
 - ⁵ B. Lounis and M. Orrit, *Rep. Prog. Phys.* **68**, 1129 (2005).
 - ⁶ O. Benson, C. Santori, M. Pelton, and Y. Yamamoto, *Phys. Rev. Lett.* **84**, 2513 (2000).
 - ⁷ R. M. Stevenson, R. J. Young, P. Atkinson, K. C. D. A. Ritchie, and A. J. Shields, *Nature* **439**, 179 (2006).
 - ⁸ N. Akopian, N. H. Lindner, E. Poem, Y. Berlatzky, J. Avron, D. Gershoni, B. D. Gerardot, and P. M. Petroff, *Phys. Rev. Lett.* **96**, 130501 (2006).
 - ⁹ N. N. Ledentsov, M. Grundmann, F. Heinrichsdorff, D. Bimberg, V. M. Ustinov, A. E. Zhukov, M. V. Maximov, and Z. I. A. J. A. Lott, *IEEE J. Select. Topic Quantum Electron* **6**, 439 (2000).
 - ¹⁰ M. Bayer, P. Hawrylak, K. Hinzer, S. and M. Korkinsinkl, Z. R. Wasilewski, O. Stern, and A. Forchel, *Science* **291**, 451 (2001).
 - ¹¹ J.-Y. Marzin, J.-M. Gérard, A. Izraël, D. Barrier, and G. Bastard, *Phys. Rev. Lett.* **73**, 716 (1994).
 - ¹² S. Yamauchi, K. Komori, I. Morohashi, K. Goshima, T. Sugaya, and T. Takagahara, *Appl. Phys. Lett.* **87**, 182103 (2005).
 - ¹³ J.-S. Tang, C.-F. Li, M. Gong, G. Chen, Y. Zou, J.-S. Xu, and G.-C. Guo, *Physica E: Low-dimensional Systems and Nanostructures* **41**, 797 (2009).
 - ¹⁴ H. Kamada, H. Gotoh, J. Temmyo, T. Takagahara, and H. Ando, *Phys. Rev. Lett.* **87**, 246401 (2001).
 - ¹⁵ X. Xu, B. Sun, P. R. Berman, D. G. S. and Allan S. Bracker and Dan Gammon, and L. J. Sham, *Nature Physics* **4**, 692 (2008).
 - ¹⁶ A. J. Shields, *Nat. Photon.* **1**, 215 (2007).
 - ¹⁷ A. Dousse, J. Suffczyński, A. Beveratos, O. K. A. Lemaitre, I. Sagnes, J. Bloch, and P. V. and P. Senellart, *Nature* **466**, 217 (2010).
 - ¹⁸ Y. H. Shih and C. O. Alley, *Phys. Rev. Lett.* **61**, 2921 (1988).
 - ¹⁹ T. E. Kiess, Y. H. Shih, A. V. Sergienko, and C. O. Alley, *Phys. Rev. Lett.* **71**, 3893 (1993).
 - ²⁰ A. Zunger, *phys stat. sol (b)* **224**, 727 (2001).
 - ²¹ L.-W. Wang, J. Kim, and A. Zunger, *Phys. Rev. B* **59**, 5678 (1999).
 - ²² L.-W. Wang and A. Zunger, *Phys. Rev. B* **59**, 15806 (1999).
 - ²³ M. Zieliński, M. Korkusiński, and P. Hawrylak, *Phys. Rev. B* **81**, 085301 (2010).
 - ²⁴ S. Lee, L. Jönsson, J. W. Wilkins, G. W. Bryant, and G. Klimeck, *Phys. Rev. B* **63**, 195318 (2001).
 - ²⁵ R. Santoprete, B. Koiller, R. B. Capaz, P. Kratzer, Q. K. K. Liu, and M. Scheffler, *Phys. Rev. B* **68**, 235311 (2003).
 - ²⁶ F. Ding, R. Singh, J. D. Plumhof, T. Zander, V. K. rápek, Y. H. Chen, M. Benyoucef, V. Zwiller, K. Dörr, G. Bester, et al., *Phys. Rev. Lett.* **104**, 067405 (2010).
 - ²⁷ R. Singh and G. Bester, *Phys. Rev. Lett.* **103**, 063601 (2009).
 - ²⁸ M. Ediger, G. Bester, A. Badolato, P. M. Petroff, K. Karrai, A. Zunger, and R. J. Warburton, *Nature Physics* **3**, 774 (2007).
 - ²⁹ M. Ediger, G. Bester, B. D. Gerardot, A. Badolato, P. M. Petroff, K. Karrai, A. Zunger, and R. J. Warburton, *Phys. Rev. Lett.* **98**, 036808 (2007).
 - ³⁰ G. Bester, S. Nair, and A. Zunger, *Phys. Rev. B* **67**, 161306 (2003).
 - ³¹ M. Gong, W. Zhang, G.-C. Guo, and L. He, *Phys. Rev. Lett.* **106**, 227401 (2011).
 - ³² V. Loo, L. Lanco, A. L. and Isabelle Sagnes, O. Krebs, P. Voisin, and Pascale Senellart, *Appl. Phys. Lett.* **97**, 2411110 (2010).
 - ³³ D. Press, S. Götzinger, S. Reitzenstein, C. Hofmann, A. Löffler, M. Kamp, A. Forchel, and Y. Yamamoto, *Phys. Rev. Lett.* **98**, 117402 (2007).
 - ³⁴ F. P. Laussy, E. del Valle, and C. Tejedor, *Phys. Rev. Lett.* **101**, 083601 (2008).
 - ³⁵ D. Englund, A. Faraon, I. Fushman, N. S. P. Petroff, and J. Vuičković, *Nature* **450**, 857 (2007).
 - ³⁶ G. Ortner, M. Schwab, M. Bayer, R. Pässler, S. Fafard, Z. Wasilewski, P. Hawrylak, and A. Forchel, *Phys. Rev. B* **72**, 085328 (2005).
 - ³⁷ M. Gong, G. Chen, L. He, C.-F. Li, J.-S. Tang, F.-W. Sun, Z.-C. Niu, S.-S. Huang, Y.-H. Xiong, H.-Q. Ni, et al., *Europhysics Letters* **90**, 37004 (2010).
 - ³⁸ I. Yeo, J. D. Song, and J. Lee, *Appl. Phys. Lett.* **99**, 151909 (2011).
 - ³⁹ S. Hameau, Y. Guldner, O. Verzele, R. Ferreira, G. Bastard, J. Zeman, A. Lemaitre, and J. M. Gérard, *Phys. Rev. Lett.* **83**, 4152 (1999).
 - ⁴⁰ V. Preisler, R. Ferreira, S. Hameau, L. A. de Vaultier, Y. Guldner, M. L. Sadowski, and A. Lemaitre, *Phys. Rev. B* **72**, 115309 (2005).
 - ⁴¹ P. N. Keating, *Phys. Rev.* **145**, 637 (1966).
 - ⁴² R. M. Martin, *Phys. Rev. B* **1**, 4005 (1970).
 - ⁴³ O. Madelung, *Semiconductors: Data Handbook 3rd Edition* (Springer, 2003).
 - ⁴⁴ S. C. Yu and H. Brooks, *Tech. Rep.*, Harvard University (1964).
 - ⁴⁵ C. Keffer, T. M. Hayes, and A. Bienenstock, *Phys. Rev. Lett.* **21**, 1676 (1968).
 - ⁴⁶ C. Keffer, T. M. Hayes, and A. Bienenstock, *Phys. Rev. B* **2**, 1966 (1970).
 - ⁴⁷ E. F. Skelton, P. L. Radoff, P. Bolsaitis, and A. Verbalis, *Phys. Rev. B* **5**, 3008 (1972).
 - ⁴⁸ C. S. Guenzer and A. Bienenstock, *Phys. Rev. B* **8**, 4655 (1973).
 - ⁴⁹ A. J. Williamson, L. W. Wang, and A. Zunger, *Phys. Rev. B* **62**, 12963 (2000).
 - ⁵⁰ M. P. Marder, *Condensed Matter Physics* (Wiley, New York, 1999).
 - ⁵¹ H. Y. Fan, *Phys. Rev.* **82**, 900 (1951).
 - ⁵² I. Vurgaftman and J. R. Meyer, *J. Appl. Phys.* **89**, 5815 (2001).
 - ⁵³ O. Madelung, *Semiconductors: Data Handbook 3rd Edition* (Springer, 2003).
 - ⁵⁴ R. Pässler, *Phys. Stat. Sol. (b)* **236**, 710 (2003).

- ⁵⁵ A. Franceschetti, H. Fu, L.-W. Wang, and A. Zunger, *Phys. Rev. B* **60**, 1819 (1999).
- ⁵⁶ A. Franceschetti and A. Zunger, *Europhys. Lett.* **50**, 243 (2000).
- ⁵⁷ S. A. Pour, B. Movaghar, and M. Razeghi, *Phys. Rev. B* **83**, 115331 (2011).
- ⁵⁸ L. He, G. Bester, and A. Zunger, *Phys. Rev. B* **70**, 235316 (2004).
- ⁵⁹ M. Gong, K. Duan, C.-F. Li, R. Magri, G. A. Narvaez, and L. He, *Phys. Rev. B* **77**, 045326 (2008).
- ⁶⁰ S.-H. Wei and A. Zunger, *Phys. Rev. B* **49**, 14337 (1994).
- ⁶¹ E. A. Zibik, L. R. Wilson, R. P. Green, G. Bastard, R. Ferreira, P. J. Phillips, D. A. Carder, J.-P. R. Wells, J. W. Cockburn, M. S. Skolnick, et al., *Phys. Rev. B* **70**, 161305(R) (2004).
- ⁶² E. A. Zibik, T. Grange, B. A. Carpenter, N. E. Porter, R. Ferreira, G. Bastard, D. Stehr, S. Winnerl, M. Helm, H. Y. Liu, et al., *Nature Materials* **8**, 803 (2009).
- ⁶³ G. Bester, D. Reuter, L. He, A. Zunger, P. Kailuweit, A. D. Wieck, U. Zeitler, J. C. Maan, O. Wibbelhoff, and A. Lorke, *Phys. Rev. B* **76**, 075338 (2007).
- ⁶⁴ E. E. Vdovin, A. Levin, A. Patane, L. Eaves, P. C. Main, Y. N. Khanin, Y. V. Dubrovskii, M. Henini, and G. Hill, *Science* **6**, 5489 (2000).
- ⁶⁵ M. Cardona, T. A. Meyer, and M. L. W. Thewalt, *Phys. Rev. Lett.* **92**, 196403 (2004).
- ⁶⁶ R. Passler, E. Griehl, H. Riepl, G. Lautner, S. B. H. Preis, W. Gebhardt, B. Buda, D. J. As, D. S. K. Lischka, K. Pappagelis, et al., *J. Appl. Phys.* **86**, 4403 (1999).
- ⁶⁷ M. Fernández, P. Prete, N. Lovergine, A. M. Mancini, R. Cingolani, L. Vasanelli, and M. R. Perrone, *Phys. Rev. B* **55**, 7660 (1997).